Materials Systems and Processes for Three Dimensional Micro- and Nanoscale Fabrication and Lithography, S. M. Kuebler and V. T. Milam, Eds, Materials Research Society, Vol. 1179E, 1179-BB08-02 (2009)

Thermocapillary Patterning of Nanoscale Polymer Films

Mathias Dietzel and Sandra M. Troian
Dept. of Applied Physics, Laboratory of Interfacial & Small Scale Transport,
California Institute of Technology 1200 E California Blvd, MC 128-95, Pasadena, CA 91125

ABSTRACT

We investigate a method for non-contact patterning of molten polymer nanofilms based on thermocapillary modulation. Imposed thermal distributions along the surface of the film generate spatial gradients in surface tension. The resulting interfacial stresses are used to shape and mold nanofilms into 3D structures, which rapidly solidify when cooled to room temperature. Finite element simulations of the evolution of molten shapes illustrate how this technique can be used to fabricate features of different heights and separation distances in a single process step. These results provide useful guidelines for controlling proximity effects during evolution of adjacent structures.

INTRODUCTION

While conventional UV lithography offers unparalleled resolution for device fabrication, there is growing interest in alternative, less costly and more rapid patterning techniques for construction of micro-optic, photonic and optoelectronic devices. It has been shown, for example, that components for MEMS devices can be fabricated more cheaply by microcontact printing, micromolding, microembossing or nanoimprinting [1,2]. Letterpress techniques have also been used to generate polymeric masks for resist-free printing of amorphous silicon thin film transistors whose performance is equivalent to those fabricated by conventional means [3,4]. Equally promising are techniques for construction of microscale components by non-contact means such as electrohydrodynamic ink-jetting [5], whereby small volumes are jetted onto selective sites of a target substrate. Our interest in inexpensive fabrication of small and large area arrays has led us to investigate an unusual method for non-contact patterning of molten polymer films which allows construction of adjacent 3D structures with different heights and spacings in one process step. Imposed thermal distributions along the surface of the film, typically enforced by proximity to a cooler master patterned substrate, generate spatial gradients in surface tension. The corresponding surface stresses elongate or depress selective regions of the film by inducing liquid flow from warmer to cooler regions. It is anticipated that structures formed from the melt in this way will exhibit superior optical performance due to the formation of specularly smooth surfaces upon solidification.

In previous work [6], we have examined what physical mechanisms are responsible for the spontaneous emergence of nanopillar arrays in experiments involving spun cast films of polymer melts subject to a large transverse thermal gradient [7-11]. In brief, the experiments consist of a spun cast molten film of polystyrene (PS) or poly(methyl methacrylate) (PMMA) of thickness h_o (80-130 nm) inserted in between two flat and parallel silicon wafers separated by a distance $d_o > h_o$ (100-600 nm) and subject to a temperature difference $\Delta T = T_2 - T_1$; both temperatures are held above the polymer glass transition temperature (approx. 100 °C) during the course of the experiment. Typically, d_o/h_o ranges from about 2–8; the critical air gap above the melt ensures a free

deformable interface. Although ΔT is rather small (10-50°C), the narrow gap establishes a large thermal gradient of order 10^6-10^8 °C/cm. Free surface films which are initially smooth and flat are observed to undergo a hydrodynamic instability, which generates self-assembling nanopillars with mean spacing approximately 1-10 μm which are drawn toward the cooler substrate. AFM images of the solidified structures reveal hexagonal, square or lamellar in-plane symmetry. Our previous analysis [4] challenged the prevailing explanation for pillar formation, which relies on modulation of a surface radiation pressure induced by internal reflection of acoustic phonons. We have shown instead that thermocapillary stresses play a critical if not dominant role in the process. Predictions of that model for the most unstable wavelength λ_{max} as a function of h_o, d_o and relevant material parameters show good agreement with actual values of the pillar spacing.

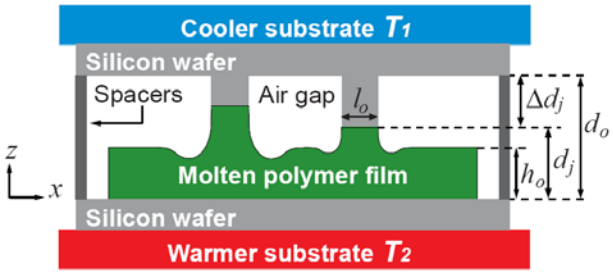

Figure 1 Schematic diagram corresponding to numerical simulations of nanofilm deformation by thermocapillary modulation. Upper wafer contains protruding elements (labeled by index j) of diameter l_o and depth d_o–d_j. In this study, h_o=100 nm, d_o=285 nm and ΔT= T_2 - T_1 = 170°C-124°C = 46°C. All remaining variables and material properties are provided in the Discussion section.

In this work, we explore the influence of a patterned upper wafer on the film shaping process. A cross-sectional view of the system corresponding to the numerical simulations is shown in Figure 1. The cooler top wafer held throughout at temperature T_1 is patterned with several protrusions of width l_o and depth Δd_j (j = 1,..,4). Thermal gradients within the silicon wafers are neglected since the thermal conductivity of silicon is three orders of magnitude larger than air or polymer. We investigate by finite element simulations wave interference effects that arise during the formation of adjacent structures. In particular, we focus on the influence of lateral feature size l_o on the number and shape of peaks formed in order to quantify proximity effects.

THEORETICAL MODEL

The derivation of the interface equation corresponding to thermocapillary flow within an ultrathin polymer film driven by thermal modulation of the polymer surface tension is lengthy and not reproduced here; the interested reader can refer to Ref. 6 for additional details. The most notable assumptions of the analysis (consistent with experiment) are as follows: (i) the polymer is modeled as a Newtonian fluid since the film shear rates are very small, (ii) the polymer viscosity is assumed constant [$\eta=\eta(T_2)$], (iii) the fluid dynamics and heat transfer are well approximated by the slender gap limit for which $\varepsilon^2 = (h_o/l_o)^2 \le (h/l_o)^2 < (d_o/l_o)^2 << 1$ and $\varepsilon Re << 1$ [12], where the Reynolds number Re is based on the initial film thickness h_o, and (iv) the heat transfer through the gas and polymer layers reduces to a 1D conduction equation along the z-axis. Variations in interfacial temperature that develop parallel to the (dimensionless) evolving interface, $H(X,Y,\tau)=h(x,y,t)/h_o$, generate tangential shear stresses, which promote the growth of pillars toward the cooler plate. Capillary forces, which repress formation of additional surface area, are incorporated through a normal stress boundary condition. The resulting evolution equation is given by:

$$\frac{\partial H}{\partial \tau} + \nabla_{\parallel} \cdot \left(\frac{\kappa \overline{Ma} H^2}{2\left[D + (\kappa - 1) H \right]^2} \left(D \nabla_{\parallel} H - H \nabla_{\parallel} D \right) + \frac{H^3}{3\,\overline{Ca}} \nabla_{\parallel}^3 H \right) = 0 \ . \qquad (1)$$

The dimensionless variables are defined by $(X,Y,Z) = (x/l_o, y/l_o, z/h_o)$, where l_o is the lateral feature size shown in Figure 1, $\nabla_{\parallel} = (\partial / \partial X, \partial / \partial Y)$, $[H, D_o, D, D_j, \Delta D_j] = [h(x,y,t)/h_o, d_o/h_o, d(x,y)/h_o, d_j/h_o, \Delta d_j/h_o]$ where $D(X,Y)$ defines the surface topology of the upper wafer, $\tau = t\, u_c/l_o$ where t is real time, $\kappa = k_{\text{air}}/k_{\text{polymer}}$ denotes the thermal conductivity ratio and $\overline{Ma} = \varepsilon \gamma_T \Delta T/(\eta u_c)$ and $\overline{Ca} = \eta u_c/(\gamma \varepsilon^3)$ denote the modified Marangoni and capillary number. Additionally, $\gamma_T = |d\gamma/dT|$ denotes the variation in surface tension with temperature, $\Delta T = T_2 - T_1$, and $u_c = (4\pi)^2 \varepsilon \gamma\, h_o^2/(3\eta \lambda_{max}^2)$ is the characteristic horizontal speed established by thermocapillary flow. All material properties are evaluated at T_2. The characteristic scale λ_{max} refers to the wavelength of the fastest growing mode obtained from linear stability analysis of pillar growth in between flat plates [6]:

$$\lambda_{max} = 2\pi h_o \sqrt{4\gamma h_o / (3\kappa d_o \gamma_T \Delta T)} \left(d_o / h_o + \kappa - 1 \right). \qquad (2)$$

As evident from Eq. (1), the evolving film thickness $H(X,Y,\tau)$ is controlled by the competition between the thermocapillary term (preceded by $\overline{Ma}$), which drives fluid toward cooler protrusions, and the capillary term (preceded by $\overline{Ca}^{-1}$), which represses formation of additional surface area. Gravitational forces are negligibly small for the nanofilms under study. In what follows, we focus on results of numerical simulations in which the topology of the top wafer is described by an array of protrusions labeled by index j of lateral extent l_o and depth $D(X,Y) = D_o - \Delta D_j F(X,Y)$ where $F(X,Y) = \{1 - \tanh[c(2\xi/l_o - 1)]\}/2$; the parameter c controls the side-wall slope of a protruding element, set to 10 in this study. For a single extended ridge, $\xi = |X|$; for a square array of four cylindrical protrusions, $\xi = [(X-X_{o,j})^2 + (Y-Y_{o,j})^2]^{1/2}$, where $(X_{o,j}, Y_{o,j})$ denotes the cylinder midpoint viewed from above. We note that Eq.(1) describes the formation of molten pillars and is therefore valid up until the moment these contact a protruding element. Subsequent spreading or solidification after contact is beyond the scope of this study since the kinetics of polymer spreading along a solid surface requires additional specification of the dynamics of moving contact lines, models of which are still under debate.

DISCUSSION

We have conducted finite element simulations [13] of Eq. (1) for two types of wafer topology to gain insight into proximity effects arising from wave interference during pattern evolution. For all studies presented except where explicitly noted, the following parameters were held fixed: h_o=100 nm, d_o=285 nm, T_2=170°C and T_1=124°C. The material constants correspond to those of PS quoted in the literature: γ= 0.0315 N/m and γ_T =0.0885 · 10^{-3} N/m-°C (at 180°C [14]), η=2.5 · 10^5 Pa-s (at 170 °C [15]) and κ=0.277 (at 170 °C [16,17]). For the configuration examined in Figure 2, the top wafer is patterned into a square array of four cylinders of diameter l_o=1 μm, which measure in depth ΔD_j (j = 1–4) = 1.25, 1.0, 0.75 and 0.50. In this case, u_c=2.84 nm/s, λ_{max} = 4.83 μm, $\overline{Ma}$ = 5.73 and $\overline{Ca}$ = 2.25. Shown in the figure are cross-sectional views along the perimeter distance S for pillar spacings ΔS = 2, 3, 4 and 5 (measured in units of l_o) at four times τ ranging from 0 to 0.145; the final time shown corresponds to contact of the polymer melt with the longest protrusion. The inset of Figure 2(b) shows 3D images of the evolving film at the prescribed times for a pillar spacing ΔS=3. The metric bar shown in (c) provides a comparison of

the spacing ΔS to the dimensionless wavelength λ_{max}/l_o=4.83. The color inset in (d) displays the variation in polymer surface temperature $\Theta(Z=H) = (T_{z=h}-T_1)/(T_2 - T_1)$ at the specified times for a pillar spacing ΔS=5. These results indicate that the time required to contact the longest protrusion is rather insensitive to ΔS; however, the longest protrusion generates the most significant film deformation, both vertically and horizontally, since the local thermal gradients are larger. The material necessary for growth of a pillar must flow from its vicinity, a process which depletes polymer from the surrounding areas to produce the characteristic dips observed on either side of the main pillar. For the shapes shown in Figure 2(a) – (d), the lateral extent of film deformation beneath the longest protrusion is approximately $4l_o$. Consequently, neighboring waveforms undergo interference for cylinder spacings less than this value, as observed in Figures 2(a) and (b). Constructive interference between neighboring perturbations also leads to steeper depressions, as shown in Figure 2(a). The amplitude and lateral extent of these oscillatory sidewaves depends on the time required for the main peak to reach the protruding surface; therefore, good temporal control is ultimately required to affix desired shapes.

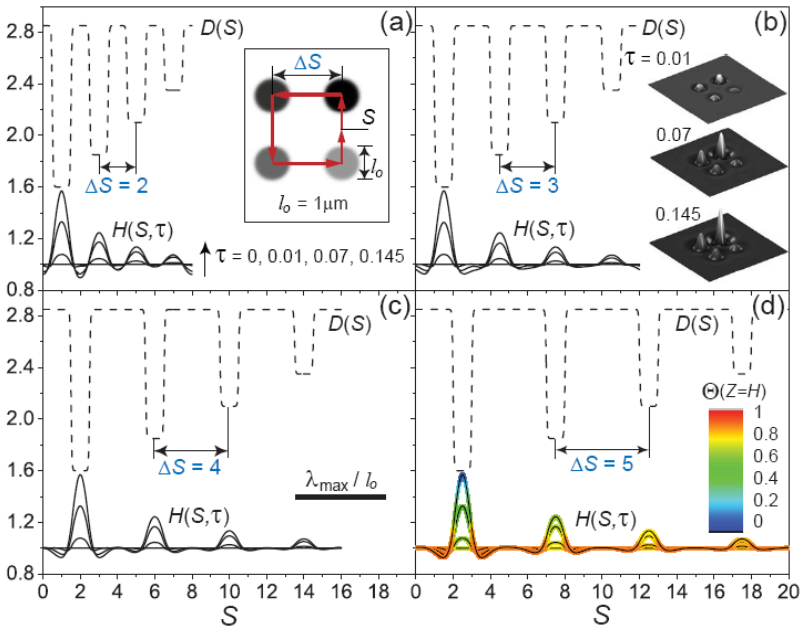

Figure 2 Plots of the film thickness $H(S,\tau)$ as a function of perimeter distance S (measured in counterclockwise fashion) as a function of time τ = 0.0, 0.01, 0.07 and 0.145 for a square array of cylindrical protrusions of diameter l_o = 1 μm and decreasing size 1.25, 1.0, 0.75 and 0.5 (in units of h_o), separated by an equal distance (a) ΔS=2, (b) ΔS=3, (c) ΔS=4, and (d) ΔS=5.

These results illustrate some of the advantages of using substrate preforms to enhance or depress selective regions of a polymer film within a single process run, in contrast to multiple steps normally required with photolithography. These simulations also reveal that for the polymer materials and temperatures of interest, the pillar formation process is surprisingly rapid. For the cases shown, the tallest peak contacts the upper protrusion in less than a minute. This rapid response is due to the fact that the local thermal gradient increases as a peak approaches the upper plate, as depicted by the colored thermal profiles shown in Figure 2(d), which leads to ever faster film evolution.

The study shown in Figure 3 demonstrates more vividly the influence on film shape caused by an imposed feature size either smaller or larger than the hydrodynamic length scale λ_{max}. Shown in Figure 3(a) is a cross-sectional view of the film shape generated by a single protrusion of depth 50 nm resembling an extended ridge with a width at half-maximum set either to 4 or 5 μm. For comparison, the corresponding instability wavelength for unpatterned wafers is λ_{max}=4.83 μm. For the smaller ridge width, the film develops a single peak centered beneath the

protrusion. For the larger ridge width, two sharp peaks develop beneath the corners of the ridge. Corresponding 3D images of the film shape are shown in Figure 3(b). For these runs, $\overline{Ma} = 5.73$ but $\overline{Ca} = 36.0$ for the smaller width (u_c = 0.71 nm/s) and $\overline{Ca} = 56.3$ for the larger width (u_c = 0.57 nm/s). Inspection of Eq. (1) reveals that the stabilizing effect of capillary forces is weakened for the wider profile, which enables the formation of two peaks. As also shown in Figure 3(b), the narrow protrusion allows the formation of a central peak with little undulation along the *Y*-axis within the time period required for the polymer to contact the protrusion. In contrast, the wider protrusion generates an instability along the peak backbone upon approach to the protruding surface. If in Eq. (2) the local gap between the bottom substrate and bottom of the ridge i.e. $d_j = 235$ nm is substituted instead of the main gap size d_o, then $\lambda_{max} = 4.07$ μm or likewise, $\lambda_{max}/l_o = 0.814$, which closely approximates the wavelength observed for the backbone instability. We are investigating whether this secondary instability may develop in response to the wider ridge width which exceeds λ_{max}. This allows the formation of two spikes of high curvature which may be subject to a Rayleigh as well as thermocapillary instability.

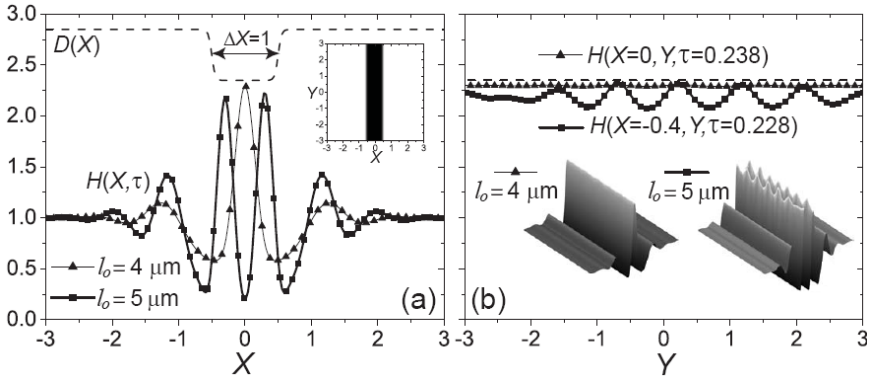

Figure 3 Results of film shapes induced by a top wafer patterned with a single extended protrusion resembling a ridge of width 4 μm or 5 μm.
(a) Cross-sectional view of film surface along the *X*-axis. (b) Cross-sectional view of film surface along the *Y*-axis. Remaining parameter values are provided in the text.

Waveform distortion can be minimized by placing protrusions in close proximity to the polymer surface. Shown in Figure 4 is an example of a protrusion similar in shape to the wider ridge in Figure 3 but for different processing parameters where h_o = 500 μm and d_o = 2 μm. The protrusion depth Δd_j and width l_o were chosen to be 1.36 μm and 5 μm, respectively. In this case, $l_o << \lambda_{max} = 31.4$ μm as given by Eq. (2). The remaining parameter values are $\overline{Ma} = 9.69$, $\overline{Ca} = 1.33$ and $u_c = 1.68$ nm/s. The lateral feature size induced in the polymer film more closely approximates the imposed pattern width, which suggests that the ultimate resolution achievable may require implementation of thermal distributions in close proximity to the polymer surface.

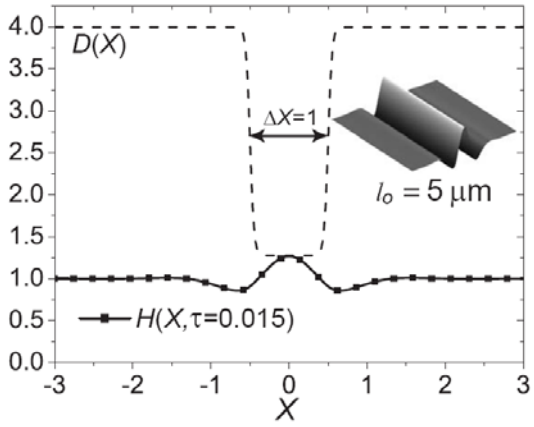

Figure 4 Film shape $H(X,\tau)$ induced by a ridge placed in close proximity to the polymer surface. The ridge width l_o is much smaller than the instability wavelength described by Eq. (2) pertinent to a flat wafer with no protrusions. Remaining parameter values are provided in the text.

The differences in feature replication observed in Figures 2 – 4 are strongly dependent on the balance between thermocapillary and capillary terms shown in Eq.(1). This amplitude ratio is given by $\Psi = 3\kappa \overline{Ma}\ \overline{Ca}\ /[2(D+\kappa\text{-}1)^2]$ for deformations $\nabla_{\|} H$ of order 1. For the parameter values in Figure 2, ψ=1.18. In Figure 3, ψ=18.9 for l_o=4 μm and ψ=29.6 for l_o=5 μm. In Figure 4, ψ=0.5. Good pattern replication is therefore achieved for smaller values of ψ and predominance of the term $\nabla_{\|} D$ in comparison to $\nabla_{\|} H$. This limit ensures that the imposed thermal gradient is imposed by the topology of the top wafer and not by subsequent deformations in film thickness.

CONCLUSION

We have demonstrated by numerical simulation some features affecting pattern fidelity and waveform interference resulting from thermocapillary shaping of nanoscale polymer films. Selective growth of individual features is made possible in one process step despite the proximity of adjacent structure formation. Thermocapillary waves induced within the molten polymer film can be made to interfere constructively or destructively depending on the distance between emerging structures. This dynamic method of film patterning requires accurate temporal control to minimize feature distortion by thermocapillary waves.

ACKNOWLEDGEMENT

We gratefully acknowledge financial support for this study from the Electrical, Communications and Cyber Systems Division of the National Science Foundation.

REFERENCES

1. L. J. Guo, Adv. Mat. **19**, 495 (2007).
2. E. Menard *et al.*, Chem. Rev. **107**, 1117 (2007).
3. S. M. Miller, S. M. Troian and S. Wagner, J. Vac. Sci. Tech. B **20**, 2320 (2002).
4. S. M. Miller, S. M. Troian and S. Wagner, Appl. Phys. Lett. **83** (15), 3207 (2003)
5. J. Park *et al.*, Nature Materials **6**, 782 (2007).
6. M. Dietzel and S. M. Troian, submitted to Phys. Rev. Lett. – see also arXiv:physics.flu-dyn http://arxiv.org/abs/0903.4899 (2009).
7. S. Y. Chou, L. Zhuang and L. J. Guo, Appl. Phys. Lett. **75**, 1004 (1999).
8. E. Schäffer *et al.*, Europhys. Lett. **60**, 255 (2002).
9. E. Schäffer *et al.*, Macromol. **36**, 1645 (2003).
10. E. Schäffer *et al.*, Adv. Mat. **15**, 514 (2003).
11. J. Peng *et al.*, Polymer **45**, 8013 (2004).
12. L.G. Leal, *Fluid Mechanics and Convective Transport Processes* (Cambridge Univ. Press, 2007).
13. COMSOL Multiphysics, V3.4, Comsol, Inc. (Los Angeles, CA, 2007).
14. J. C. Moreira and N. R. Demarquette, J. Appl. Polym. Sci. **82**, 1907 (2001).
15. J. L. Masson and P. F. Green, Phys. Rev. E **65**, 31806 (2002).
16. D. R. Lide, *CRC Handbook of Chem. and Phys.*, 73rd ed. (CRC Publ. Co., Boca Raton, Fl., 1992).
17. J.E. Mark, *Physical Properties of Polymers Handbook* (AIP Press, Woodbury, NY, 1996).